PCCP

PAPER

View Article Online
View Journal | View Issue

Cite this: *Phys. Chem. Chem. Phys.*, 2024, **26**, 6646

Kinetics of the reaction of OH with methyl nitrate (223–343 K)†

Christin Fernholz, Fabienne Baumann, Jos Lelieveld and John N. Crowley *

Received 5th January 2024,
Accepted 1st February 2024

DOI: 10.1039/d4cp00054d

rsc.li/pccp

Rate coefficients (k_4) for the reaction of hydroxyl radicals (OH) with methyl nitrate (CH_3ONO_2) were measured over the temperature range 232–343 K using pulsed laser photolysis to generate OH and pulsed laser-induced fluorescence to detect it in real-time and under pseudo-first-order conditions. In order to optimize the accuracy of the rate coefficients obtained, the concentration of CH_3ONO_2 (the reactant in excess) was measured on-line by absorption spectroscopy at 213.86 nm for which the absorption cross-section was also measured ($\sigma_{213.86}$ = 1.65 ± 0.09 × 10^{-18} cm^2 molecule^{-1}). The temperature-dependent rate coefficient is described by $k_4(T)$ = 7.5 × 10^{-13} exp[(−1034 ± 40)/T] cm^3 molecule^{-1} s^{-1} with a room temperature rate coefficient of k_4(296 ± 2 K) = (2.32 ± 0.12) × 10^{-14} cm^3 molecule^{-1} s^{-1} where the uncertainty includes the statistical error of 2σ and an estimation of the potential systematic bias of 5%. This new dataset helps to consolidate the database for this rate coefficient and to reduce uncertainty in the atmospheric lifetime of CH_3ONO_2. As part of this study, an approximate rate coefficient for the reaction of H-atoms with CH_3ONO_2 (k_9) was also derived at room temperature: k_9(298 K) = (1.68 ± 0.45) × 10^{-13} cm^3 molecule^{-1} s^{-1}.

1 Introduction

Organic nitrates are formed in the atmosphere during the degradation of hydrocarbons in the presence of nitrogen oxides.[1] The atmospheric lifetimes of organic nitrates can vary from seconds (*e.g.* for thermally unstable peroxy-nitrates such as CH_3OONO_2 at temperatures close to room temperature) to months (*e.g.* for α-carbonyl peroxy-nitrates such as $CH_3C(O)OONO_2$ at temperatures close to 220 K typical for the upper troposphere). In contrast to peroxy-nitrates, alkyl nitrates (such as CH_3ONO_2) are generally thermally stable at the temperatures of our atmosphere and can be transported over long distances before being oxidized *via* reaction with OH or photolyzed.[1–3] Following OH-induced oxidation of hydrocarbons, alkyl nitrates are formed in a usually minor (termolecular) channel of the reaction of organic peroxy radicals (RO_2) with NO:

$$RO_2 + NO \rightarrow RO + NO_2 \quad (R1a)$$

$$RO_2 + NO + M \rightarrow RONO_2 + M \quad (R1b)$$

Alternatively, $RONO_2$ can be formed in the NO_3-induced oxidation of unsaturated biogenic hydrocarbons in the presence of O_2, which involves electrophilic addition of NO_3 to a C=C double bond followed by further reaction of the nitro-peroxy radicals thus formed.[4] The target molecule of this study, CH_3ONO_2 is formed in the lower atmosphere when CH_3O_2 radicals (*e.g.* from methane oxidation) react with NO. The formation of CH_3ONO_2 *via* this reaction is inefficient, with a yield of <1% at room temperature,[5] but with some evidence for an increase in the yield at lower temperatures, commensurate with its formation in a termolecular process:[6]

$$CH_3O_2 + NO \rightarrow CH_3O + NO_2 \quad (R2a)$$

$$CH_3O_2 + NO + M \rightarrow CH_3ONO_2 + M \quad (R2b)$$

In the lower atmosphere, the fate of CH_3O is dominated by reaction with O_2 to form HO_2 and HCHO. However, in the stratosphere, when O_2 concentrations are much lower, some CH_3O can react with NO_2[7] and this represents a further source of CH_3ONO_2:

$$CH_3O + NO_2 + M \rightarrow CH_3ONO_2 + M \quad (R3)$$

The important chemical loss processes for CH_3ONO_2 in the atmosphere are photodissociation and reaction with OH, with thermal decomposition and reaction with O_3 or NO_3 insignificant.[1,8] Previous measurements indicate that R4 has a small rate coefficient, of the order of 10^{-14} cm^3 molecule^{-1} s^{-1} (see below). The photolysis of CH_3ONO_2 proceeds *via* O–N bond fission to form a methoxy radical and NO_2, whereas the slow reaction with OH (R4) proceeds *via* H-abstraction to form an unstable radical that dissociates to formaldehyde and NO_2(R5):

Atmospheric Chemistry Department, Max Planck Institute for Chemistry, Mainz 55128, Germany. E-mail: john.crowley@mpic.de

† Electronic supplementary information (ESI) available. For ESI and crystallographic data in CIF or other electronic format see DOI: https://doi.org/10.1039/d4cp00054d

$$OH + CH_3ONO_2 \rightarrow CH_2ONO_2 + H_2O \quad (R4)$$

$$CH_2ONO_2 \rightarrow HCHO + NO_2 \quad (R5)$$

Both HCHO and CH_3O react much more rapidly with OH than does CH_3ONO_2 and secondary chemistry is a potential source of systematic bias in the determination of the rate coefficient (k_4) for the title reaction when using absolute rate methods. A further source of systematic bias in an absolute rate coefficient study of this slow reaction (R4) is the presence of reactive impurities in the CH_3ONO_2 sample. Such problems can be avoided by working at low OH concentrations (and thus low fractional conversion of CH_3ONO_2 to products) and by carefully purifying the CH_3ONO_2 sample, thus minimising the levels of reactive impurities (see Section 2).

The rate coefficient for reaction (R4) has been reported by Gaffney *et al.*,[9] Nielsen *et al.*,[10] Talukdar *et al.*,[8] and Shallcross *et al.*,[11] but there are large differences in the rate coefficient at room temperature (a factor of 10) and its temperature dependence which is reported to be both positive and negative (see later). The goal of this study is to generate highly accurate rate coefficients for the title reaction at different (atmospherically relevant) temperatures and to resolve these differences in the literature and thus better constrain the lifetime of CH_3ONO_2 in the atmosphere.

2 Experimental

Rate coefficients for the reaction of OH with CH_3ONO_2 were determined using pulsed-laser-photolysis (PLP) pulsed-laser-induced fluorescence (PLIF) under pseudo-first-order conditions ($[CH_3ONO_2] \gg [OH]$) in (mainly) N_2 and He bath gases. The concentration of methyl nitrate was measured *in situ* by optical absorption. The experimental setup has been described in detail elsewhere[12] and is only briefly described here.

2.1 PLP–PLIF technique

The reaction took place in a cylindrical, jacketed quartz reactor with a volume of approximately 300 cm^3. The temperature inside the reactor was controlled by circulating a 60 : 40 ethylene glycol/water mixture (343–251 K) or ethanol ($T < 251$ K) through an outer-jacket. The gas mixture enters the reactor about 15 cm before the photolysis zone, ensuring thermal equilibrium with the walls of the reactor. The reaction temperature was measured by inserting a recently calibrated K-type thermocouple into the photolysis zone before each experiment at a different temperature. 100 and 1000 torr manometers were used to measure the pressure in the reactor.

OH was generated by excimer laser photolysis (Coherent COMPex 205 F or Pro 201 F, ~20 ns width) of a precursor gas molecule, either H_2O_2 (248 nm), HONO (351 nm) or CH_3ONO_2 itself (248 nm) (see below).

OH radicals were excited at 281.997 nm ($A^2\Sigma(\nu' = 1) \leftarrow X^2\Pi(\nu'' = 0)$, Q_{11} (1) transition) using a Nd-YAG pumped (532 nm, ~6 ns pulse width) and frequency-doubled dye laser (Quantel Brilliant B, Lambda Physik Scanmate/Scanmate UV with KPD crystal). The resulting fluorescence signal was detected by a photomultiplier tube screened by a long-pass filter ($\lambda > 290$ nm). The photolysis and excitation lasers were mainly operated at a repetition rate of 10 Hz using a pulse/delay generator (Stanford Research Systems DG 535), which was also used to control the delay between the photolysis and excitation laser pulses. Prior to the PLP pulse, 20 pulses of the PLIF laser were used to measure a background signal that includes scattered light from the excitation laser and electronic noise. The averaged background signal was subtracted before further processing of the measured data. Each datapoint was averaged between 10 and 40 times, depending on the measurement.

The total flow and pressure in the reactor were chosen such that an average, linear gas-velocity of ≈13–19 cm s^{-1} was achieved, ensuring that the gas in the photolysis region was replenished between laser pulses. For measurements in helium, the linear velocity was 5 or 6.6 cm s^{-1} and the laser repetition rate was reduced to 5 Hz, to ensure complete gas exchange.

2.2 *In situ* absorption spectroscopy: The absorption cross-section of CH_3ONO_2 at 213.86 nm

As the experiments were performed under pseudo first order conditions, accurate rate coefficients depend on accurate measurement of the concentration of the excess reactant. The concentration of methyl nitrate was therefore determined on-line, downstream of the reactor by optical absorption using a dual-beam absorption cell (path length 34.8 cm) equipped with a low-pressure Zn-lamp and interference filter (214 ± 5 nm) to isolate the 213.86 nm line. The temperature (close to room temperature) and pressure (a few percent lower than in the reactor) in the absorption cell were also measured and used to make corrections for gas-density differences in the reaction and absorption cell. Optical density (OD) due to CH_3ONO_2 was converted to a concentration using the Beer–Lambert expression (1) and an absorption cross-section that was determined as described below.

$$OD = \ln(I_0/I) = \sigma_{213.86}\, l\, [CH_3ONO_2] \quad (1)$$

$\sigma_{213.86}$ is the CH_3ONO_2 absorption cross-section (cm^2 $molecule^{-1}$), l is the absorption path-length and I_0 and I are the transmitted light intensity without and with absorber, respectively and $[CH_3ONO_2]$ is the concentration of methylnitrate (molecule cm^{-3}).

To measure the absorption cross-section, the absorption cell was first filled with N_2 to determine I_0. Subsequently, static samples of CH_3ONO_2 in N_2 at different pressures were introduced into the cell from a storage bulb and the optical absorption was recorded. Two different storage bulbs (0.482% and 0.728%) made up using samples of CH_3ONO_2 from two different syntheses (≈ one month apart in time) were used to check for reproducibility. The storage bulbs were prepared using standard manometric methods with 10 and 1000 torr capacitance manometers with quoted accuracies of better than 1‰.

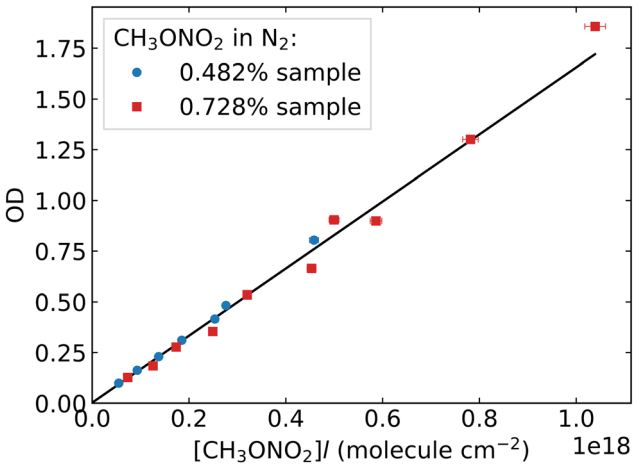

Fig. 1 Optical density (OD) plotted against concentration of methyl nitrate (molecule cm^{-3}) multiplied by path length l (cm). The slope of the corresponding, weighted linear regression yields an effective absorption cross-section of $\sigma^{213.86}_{CH_3ONO_2} = (1.65 \pm 0.09) \times 10^{-18}$ cm^2 $molecule^{-1}$. The error is 2σ and includes an estimate of systematic uncertainty.

Fig. 1 presents the results from 17 determinations of optical density at room-temperature. The slope of the weighted, linear regression gives an absorption cross-section of $\sigma_{213.86} = (1.65 \pm 0.09) \times 10^{-18}$ cm^2 $molecule^{-1}$, where the uncertainty is 2σ and includes as assessment of systematic bias (2%) which stems predominantly from uncertainty in the CH_3ONO_2 mixing ratio and thus $[CH_3ONO_2]$. In addition, minor contributions stem from uncertainty in the optical path-length (<1%) and in determination of the optical density (0.05–1.5%). As an interference filter with a finite FWHM was used to isolate the 213.86 nm Zn-line, our cross-section should strictly be regarded as an "effective" cross-section since weaker atomic lines may also be detected. Our cross-section is significantly larger than the value of 3.04×10^{-19} cm^2 $molecule^{-1}$ at 213.99 nm reported by Taylor *et al.*[13] but is similar to a value of 2.16×10^{-18} cm^2 $molecule^{-1}$ at 214.01 nm measured by McMillan *et al.* and reported by Calvert and Pitts.[14] More importantly, our value is in excellent agreement with the more recent determination of Talukdar *et al.*,[15] who obtained $\sigma_{213.86} = (1.67 \pm 0.08) \times 10^{-18}$ cm^2 $molecule^{-1}$ using a Zn-lamp. We conclude that our cross-section is approriate for converting *in situ* optical density measurements to accurate concentrations of CH_3ONO_2.

2.3 Determination of impurities in the CH_3ONO_2 sample

As the reaction between CH_3ONO_2 and OH is slow, the presence of reactive impurities can bias the rate coefficients obtained to higher values. Likely impurities are CH_3OH and HNO_3 which are involved in the synthesis of CH_3ONO_2 as well as NO_2 and HONO. Initial measurements revealed the presence of low levels of HNO_3 in the CH_3ONO_2 samples. In order to eliminate this (and other acidic gases) the sample flow was passed through ≈20 cm of PFA tubing containing nylon before entering the reactor. In some experiments (in which methyl nitrate itself was used as OH source) $CaCO_3$ was used to remove HNO_3.

Table 1 Impurities and their contribution to the OH decay coefficient

Impurity	Fraction[a]	$k_{impurity}$[b]	Contribution to k' (%)
HNO_3	<0.01	1.5×10^{-13}	<0.06
CH_3OH	<0.01	9.0×10^{-13}	<0.38
HONO	<0.03	6.0×10^{-12}	<6.80
NO_2	<0.03	4.2×10^{-12}[c]	<4.78

[a] Relative concentration of impurity (in %) of the CH_3ONO_2 concentration. [b] Rate coefficient (cm^3 $molecule^{-1}$ s^{-1}) at room temperature. [c] Calculated for a pressure of 135 torr.

Following each new synthesis of CH_3ONO_2, levels of HNO_3, HONO, CH_3OH and NO_2 were determined using a combination of IR and UV/Vis absorption spectroscopy. An FTIR (Bruker Vector 22) spectrometer coupled to an absorption cell of 45 cm pathlength[16] and equipped with an external MCT detector was used to determine impurity levels of HNO_3 and CH_3OH in a flowing mixture of CH_3ONO_2 in N_2, as used in the kinetic experiments. Generally, 32 spectra at a resolution of 1 cm^{-1} (acquisition time ≈ 1 min) were co-added to measure absorption in the 700–3750 cm^{-1} range. HONO and NO_2 impurities were investigated using multi-pass (l = 880 cm) UV/Vis absorption spectroscopy (346–518 nm) using a H4-lamp light source coupled to a CCD detector (Andor DU420A-OE) and a 0.5 m monochromator (BM50) with 300 lines mm^{-1} grating. The spectral resolution (FWHM of a Hg line from a low-pressure discharge lamp) was 0.5 nm.

The results of the impurity determinations (none were detected and upper limits were established) are summarized in Table 1, which shows that the rate coefficients obtained were not significantly influenced by impurities in the CH_3ONO_2 sample.

2.4 OH sources

During the course of this study, three different sources of OH were tested. The photolysis of HONO at 351 nm (R6) and the photolysis of H_2O_2 at 248 nm (R7) both generate OH in the ground vibrational state.[17] The photolysis of CH_3ONO_2 at 248 nm is an indirect source of OH[15] *via* formation of H atoms (R8b) and (R9).

$$HONO + h\nu\ (351\ nm) \rightarrow OH + NO \quad (R6)$$

$$H_2O_2 + h\nu\ (248\ nm) \rightarrow 2OH \quad (R7)$$

$$CH_3ONO_2 + h\nu\ (248\ nm) \rightarrow CH_3O + NO_2 \quad (R8a)$$

$$CH_3ONO_2 + h\nu\ (248\ nm) \rightarrow H + CH_2ONO_2 \quad (R8b)$$

$$H + CH_3ONO_2 \rightarrow OH + CH_3ONO \quad (R9)$$

In Section 3.2 and 3.3, we describe how the OH-decays obtained using the 248 nm photolysis laser (*i.e.*, (R7) or (R8b) and (R9)) are strongly influenced by secondary reactions involving CH_3O and NO_2 resulting from the photolysis of CH_3ONO_2. Only data obtained using the photolysis of HONO at 351 nm (a wavelength at which CH_3ONO_2 no longer absorbs significantly) were used to derive the rate coefficient for the title reaction.

2.5 Chemicals

The synthesis of CH_3ONO_2, the nitration of methanol with HNO_3, was carried out according to Black and Babers[18] but with a modification of the purification step. ~62 mL of Nitric acid (HNO_3; Sigma-Aldrich, ≥65%) was pre-cooled (ice bath) in a 250 ml Erlenmeyer flask. ~31 mL of Methanol (CH_3OH; Sigma-Aldrich, ≥99.9%) was pre-cooled in a 100 mL Erlenmeyer flask. ~62 mL of sulphuric acid (Roth, 98%) was added to the nitric acid. The remaining sulphuric acid was added to the methanol using a dropping funnel with vigorous stirring, whereby a temperature of 14 °C was not exceeded. The CH_3OH/H_2SO_4 mixture was then added. The temperature of the mixture increased to about 45 °C and was subsequently kept between 32 °C and 35 °C for about 15 minutes. The mixture was then rapidly cooled in an ice-water bath for 5 minutes and then transferred to a separating funnel. The aqueous phase and part of the organic phase were discarded.

The unwashed methyl nitrate was transferred to a bubbler and N_2 was bubbled through the liquid for about 15 min to remove any dissolved methanol. The liquid was then vacuum-distilled through a drying tube with $CaCl_2$ (Roth, ≥94%, dehydrated) before the transmitted gas was trapped in a cold-finger at liquid nitrogen temperature. The methyl nitrate was then subjected to repeated freeze–pump–thaw cycles at −196 °C. Nitrogen (N_2, Air-Liquide, 99.999%) and helium (He, Westfalen, 99.999%) were used as buffer gases in the experiments. HONO was prepared *in situ* by adding 5–10 drops of 0.1 M $NaNO_2$ solution (Roth, ≥98%) into a 20 wt% H_2SO_4 solution (Roth, 98%). Hydrogen peroxide (H_2O_2; AppliChem, 35%) was vacuum distilled to >90% purity.

3 Results and discussion

In all experiments, the methyl nitrate concentration was 5–6 orders of magnitude larger than that of OH (typically 1×10^{10} molecule cm^{-3}) and pseudo-first order conditions prevailed. The decay of OH can therefore be described by

$$[OH]_t = [OH]_0 \exp(-k't) \quad (2)$$

where $[OH]_t$ is the OH concentration at time t after the photolysis laser pulse, $[OH]_0$ is the initial OH concentration and k' is the first-order decay coefficient. The latter is defined as:

$$k' = k_4[CH_3ONO_2] + k_d \quad (3)$$

where k_4 is the bimolecular rate coefficient (cm^3 $molecule^{-1}$ s^{-1}) of the reaction of methyl nitrate with OH and k_d (s^{-1}) accounts for diffusion of OH from the detection zone and its reaction with H_2O_2 or HONO.

3.1 Generation of OH from HONO photolysis at 351 nm

Fig. 2 shows an example of the OH fluorescence signal plotted against time after the excimer laser pulse. The typical HONO concentration in this experiment is approx. 1.5×10^{13} molecule cm^{-3}, which results in an initial OH concentration of ~1×10^{10} molecule cm^{-3}. As expected (eqn (2)), the decay of OH is exponential (over 2 orders of magnitude). Decay coefficients (k', s^{-1}), obtained by least-squares-fitting of eqn (2) to the OH-decays, are plotted against the respective concentration of CH_3ONO_2 in Fig. 3. A linear dependence of k' on the CH_3ONO_2 concentration (eqn (3)) was observed under all experimental conditions, enabling derivation of $k_4(T)$. Variability in the y-axis intercept of ~200–250 s^{-1} reflects slight changes in the HONO concentration between experiments at different temperatures. Prior experiments indicate that the contribution of diffusion to k' is *circa* 50–100 s^{-1}, depending mainly on the pressure (or bath gas) and the flow rate. As the rate coefficient for the reaction between OH and HONO is 6.0×10^{-12} cm^3 $molecule^{-1}$ s^{-1}

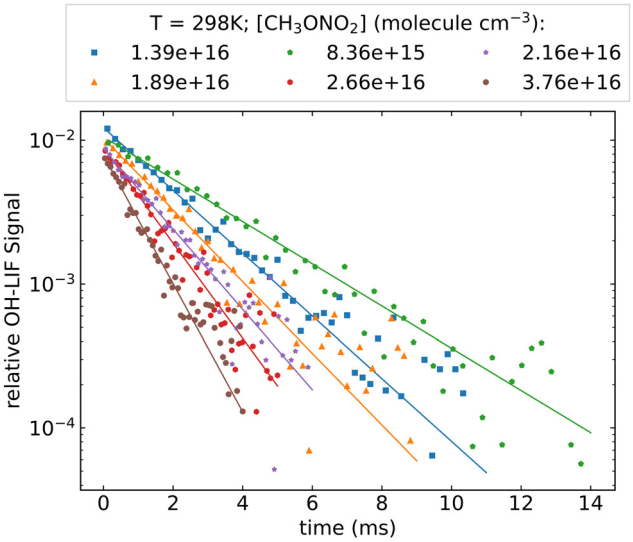

Fig. 2 OH-LIF signal (datapoints) with mono-exponential fits (solid lines) plotted against time after the photolysis laser pulse. Data were obtained using HONO as OH source at room temperature, the pressure was 134.0 torr (N_2 bath-gas).

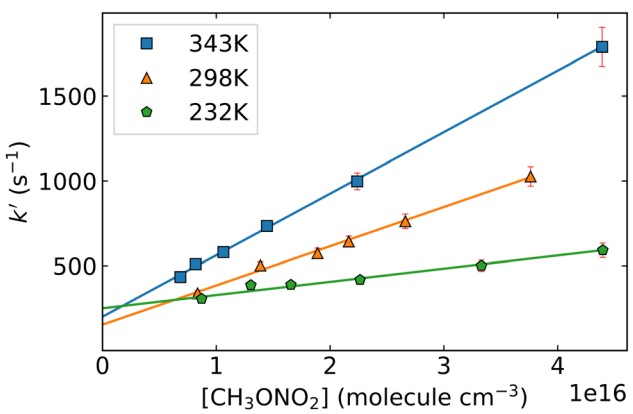

Fig. 3 First-order OH decay-coefficient (k') plotted against the corresponding methyl nitrate concentration [CH_3ONO_2] (data obtained using HONO as the OH precursor). The slope of the linear regression (orange: k(298 K) = (2.31 ± 0.15) × 10^{-14} cm^3 $molecule^{-1}$ s^{-1}; green: k(232 K) = (7.78 ± 0.92) × 10^{-15} cm^3 $molecule^{-1}$ s^{-1}; k(343 K) = (3.62 ± 0.22) × 10^{-14} cm^3 $molecule^{-1}$ s^{-1}) is the rate coefficient k_4 under these experimental conditions. Error bars represent 2σ statistical uncertainty.

Table 2 Experimental conditions and rate coefficients (k_4) for the reaction OH + CH_3ONO_2

T (K)	p (torr)	k_4 (10^{-14} cm^3 molecule^{-1} s^{-1})	Δk_4[a] (10^{-14} cm^3 molecule^{-1} s^{-1})	Bath gas
223.3	101.2	0.84	0.07	He
231.7	134.6	0.78	0.09	N_2
239.6	134.3	0.87	0.09	N_2
247.3	135.7	1.05	0.10	N_2
251.5	134.8	1.28	0.05	N_2
259.7	127.0	1.42	0.07	N_2
266.0	136.3	1.49	0.10	N_2
268.7	135.2	1.56	0.10	N_2
276.2	134.8	1.69	0.09	N_2
282.2	135.1	1.86	0.12	N_2
289.0	135.1	2.07	0.15	N_2
294.2	101.6	2.28	0.11	He
294.5	135.5	2.21	0.20	N_2
295.2	98.8	2.14	0.13	N_2
295.8	133.5	2.39	0.08	N_2
296.2	99.1	2.41	0.15	N_2
296.7	201.0	2.48	0.15	N_2
297.5	135.1	2.34	0.17	N_2
297.7	400.4	2.12	0.30	N_2
298.0	134.0	2.31	0.15	N_2
298.2	68.5	2.23	0.18	N_2
317.8	135.2	2.78	0.19	N_2
342.7	135.4	3.62	0.22	N_2

Notes: All rate coefficients were obtained using the 351 nm photolysis of HONO as OH-source. [a] Uncertainty is 2σ, statistical only.

(at room temperature), the approximate HONO concentration can be calculated to be $< 4 \times 10^{13}$ molecule cm^{-3}. This is consistent with the concentration obtained using the weak absorption (OD $< 1 \times 10^{-3}$) observed at 213.86 nm (σ = 1.8×10^{-18} cm^{-3} molecule[5]) when adding HONO in the absence of CH_3ONO_2.

Within experimental uncertainty, variation of the pressure or bath-gas (N_2 or He) (for a given temperature) had no effect on the rate coefficient, which is thus independent of pressure or collision partner within the range of pressures (69–400 torr N_2, 100 torr He) investigated in this study. Variation of the excimer-laser fluence over a factor 30 also had no significant influence (±3%) on the OH decay coefficient, showing that reactions of OH with primary and secondary products of the title reaction do not contribute significantly to its loss. A complete list of the values of k_4 obtained under various experimental conditions is given in Table 2 and plotted in Arrhenius form in Fig. 4. The regression through the data points is described by $k_4(T) = 7.5 \times 10^{-13}$ exp[(−1034 ± 40)/T]. The average, room-temperature (296 ± 2) K rate coefficient is 2.32×10^{-14} cm^3 molecule^{-1} s^{-1}. The total uncertainty associated with the rate coefficients obtained (and derived from the Arrhenius expression), is dominated by uncertainty in the concentration of CH_3ONO_2 and is estimated to be ∼ 5% (see ESI,† Section S4).

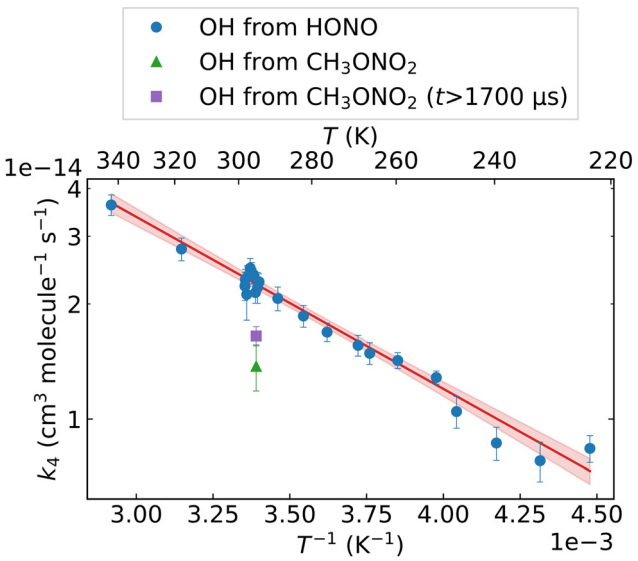

Fig. 4 Arrhenius plot of k_4 *versus* inverse temperature. In blue: k_4 from generation of OH from HONO photolysis at 351 nm. In red, the exponential fit to the data with 2σ confidence limit. In green: k_4 from generation of OH from CH_3ONO_2 photolysis at 248 nm. In purple: k_4 from generation of OH from CH_3ONO_2 photolysis at 248 nm considering only data at $t > 1.7$ ms.

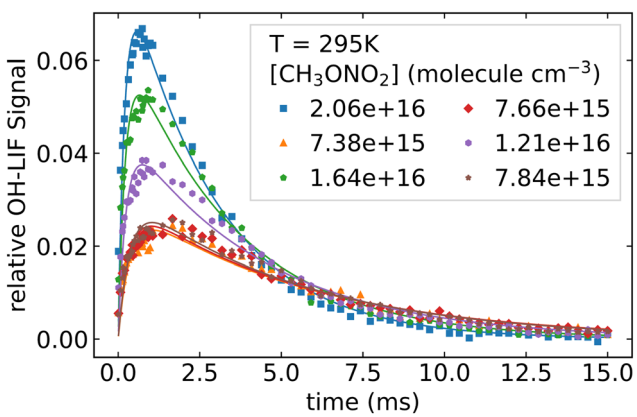

Fig. 5 OH formation and decay when different concentrations of CH_3ONO_2 were photolyzed at 248 nm.

3.2 Generation of OH from CH_3ONO_2 or H_2O_2 photolysis at 248 nm (298 K)

As described above, the photolysis of methyl nitrate at 248 nm indirectly produces OH. Based on the CH_3ONO_2 concentration, the laser fluence and the photolysis quantum yields at 248 nm,[15] between 8×10^8 and 2×10^9 molecule cm^{-3} of OH are generated *via* R8 and R9 when [CH_3ONO_2] is varied from 7.4×10^{15} to 2.1×10^{16} molecule cm^{-3}. At the same time 1.4×10^{11} to 3.9×10^{11} molecule cm^{-3} of NO_2 and CH_3O are formed.

Fig. 5 displays OH time profiles from the photolysis of six different concentrations of CH_3ONO_2. The OH decays are bi-exponential, with well separated production and loss terms. The rapid production of OH (*via* R9) is followed by a slower decay as OH is lost (mainly) *via* R4. The solid lines are fits to the data according to:

$$[OH]_t = [CH_3ONO_2]_0 \frac{k'_9}{k'_4 - k'_9}\left(\exp(-k'_9 t) - \exp(-k'_4 t)\right) \quad (4)$$

where k'_9 is the pseudo-first order term dominated by H-atom loss *via* its reactions with CH_3ONO_2(R9). In principle, values of k_4 and k_9 can be extracted from the data by plotting k'_4 and k'_9 *versus* the concentration of CH_3ONO_2 as displayed in Fig. 6. From the regression slopes we derive $k_4(298\ K) = (1.37 \pm 0.19) \times 10^{-14}$ and $k_9(298\ K) = (1.68 \pm 0.45) \times 10^{-13}$ cm^3 molecule^{-1} s^{-1}. The *y*-axis intercept of 75 ± 22 s^{-1} for the plot of k'_4 *versus* [CH_3ONO_2] is consistent with diffusive losses of OH. The much larger intercept for the plot of k'_9 *versus* [CH_3ONO_2] stems from H-atom diffusion and possibly reaction of H atoms with O_2 present as impurity.

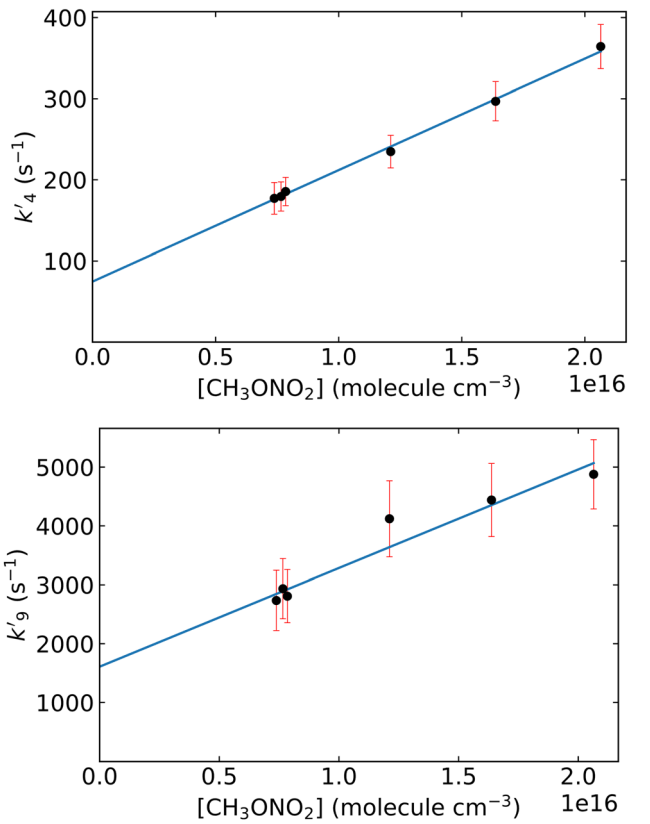

Fig. 6 First-order rate coefficients k' for OH generation and loss derived from the bi-exponential fits (eqn (4)) to OH profiles obtained by photolysis of CH_3ONO_2 at 248 nm and plotted against the corresponding methyl nitrate concentration [CH_3ONO_2] in molecule cm^{-3}. Error bars represent 2σ statistical uncertainty. The solid lines are linear regressions where the slopes correspond to the rate coefficients k_4 (upper panel) and k_9 (lower panel).

The value of k_4 thus obtained is a factor ≈ 1.6 lower than the average room-temperature value (2.32×10^{-14} cm^3 molecule^{-1} s^{-1}) obtained in the experiments in which OH was generated by the 351 nm photolysis of HONO. A different data treatment, in which only the latter part of the bi-exponential profile ($t > 1700$ μs) was analysed (*i.e.* after all H atoms have been converted to OH *via* reaction with CH_3ONO_2) results in a rate coefficient of (1.65 ± 0.10) $\times 10^{-14}$ cm^3 molecule^{-1} s^{-1}, which is also lower (factor 1.4) than that obtained using HONO photolysis. As the photolysis of CH_3ONO_2 at 248 nm results mainly in the formation of CH_3O and NO_2 and OH reacts rapidly with both (k(OH + NO_2) = 3.6×10^{-12} cm^3 molecule^{-1} s^{-1} [5] and k(OH + CH_3O) = 3×10^{-11} cm^3 molecule^{-1} s^{-1} [19] at 298 K and 100 torr), the unavoidable presence of CH_3O and NO_2 would be expected to result in an overestimation of the rate coefficient *via* this method. In the ESI† we use numerical simulations to examine the impact of secondary reactions and the effect of simultaneous detection of both OH and CH_3O (resulting in "OH" profiles that are not perfectly bi-exponential). Clearly, the photolysis of CH_3ONO_2 with complex secondary chemistry does not lend itself to accurate measurement of the OH-rate coefficient. As shown in Fig. 6, the linear relationship between k'_9 and [CH_3ONO_2] enables us to derive an approximate rate coefficient (k_9) for the OH-forming reaction of H + CH_3ONO_2. Our result is $k_9(298\ K)$ = (1.68 ± 0.45) $\times 10^{-13}$ cm^3 molecule^{-1} s^{-1}, where the uncertainty is 2σ, statistical only. This result is in good agreement with that reported by Talukdar *et al.*[15] using an almost identical method and similar analysis.

The photolysis of H_2O_2 is commonly used as a source of prompt OH radicals in PLP–PLIF experiments. The generation of OH *via* 248 nm photolysis of H_2O_2 in the presence of CH_3ONO_2 does however not result in exponential OH decays. The more complex behaviour compared to that observed when using HONO at 351 nm as OH precursor is related to the photolysis of CH_3ONO_2 at 248 nm (see above). Values of k' obtained using this method were strongly dependent on the 248 nm pulse energy and no linear relationship with the concentration of methyl nitrate was found. Clearly, as described above for experiments in the absence of H_2O_2, the photolysis of methyl nitrate at 248 nm precludes a straightforward analysis of the OH-profiles thus obtained.

3.3 Comparison of k_4 with literature values and the CH_3ONO_2 atmospheric lifetime

The low rate coefficient for the reaction of OH with CH_3ONO_2 is consistent with the reaction proceeding *via* H-atom abstraction from the methyl group, with each C–H bond contributing about 1×10^{-14} cm^3 molecule^{-1} s^{-1} to the rate coefficient at room

Table 3 Comparison with previous determinations of k_4

Source	k_4 (cm^3 $molecule^{-1}$ s^{-1})	T (K)	Method
This work	$(2.32 \pm 0.04) \times 10^{-14}$	296 ± 2	PLP–PLIF
	$7.5 \times 10^{-13} \times \exp[(-1034 \pm 40)/T]$	223–343	
Gaffney *et al.*[9]	$(3.4 \pm 0.4) \times 10^{-14}$	298	DF-RF
Nielsen *et al.*[22]	$(3.2 \pm 0.5) \times 10^{-13}$	298 ± 2	PR-RA
	$8.8 \times 10^{-15} \times \exp[(1050 \pm 180)/T]$	298–393	
	$(3.1 \pm 0.7) \times 10^{-13}$	298 ± 2	RR
Talukdar *et al.*[8]	$(2.36 \pm 0.16) \times 10^{-14}$	298	PLP–PLIF
	$8.2 \times 10^{-13} \times \exp[(-1020 \pm 60)/T]$	221–414	
Shallcross *et al.*[23]	$(4.7 \pm 1.0) \times 10^{-14}$	298	DF-RF
	$4.1 \times 10^{-13} \times \exp[(-604 \pm 121)/T]$	298–423	
Kerr and Stocker[20]	$(3.8 \pm 1.0) \times 10^{-13}$	303 ± 2	RR
Kakesu *et al.*[3]	$(3.0 \pm 0.7) \times 10^{-14}$	307 ± 3	RR

PLP–PLIF = Pulsed laser photolysis/pulsed laser induced fluorescence; DF-RF = discharge flow/resonance fluorescence; PR-RA = pulse radiolysis/resonant absorption; RR = relative rate.

temperature. Kinetic isotope effects[8] confirm that H-atom abstraction is the only significant pathway for the title reaction in the temperature range representative of our atmosphere.

In order to compare our rate coefficients and their temperature dependence with literature values, we consider only our data measured using the photolysis of HONO at 351 nm, which are not biased by complex secondary processes involving photo-fragments of CH_3ONO_2. Table 3 and Fig. 7 compare the room temperature rate coefficients and Arrhenius expression obtained in this work with those reported in the literature.

Absolute rate coefficient measurements. When considering only those studies that used absolute methods, our room-temperature rate coefficient is essentially identical to that of Talukdar *et al.*,[8] but factors of 13, 1.4 and 2 lower than those reported by Nielsen *et al.*,[10] Gaffney *et al.*[9] and Shallcross *et al.*,[11] respectively. For slow reactions such as OH + CH_3ONO_2, reactive impurities and secondary reactions of OH (*e.g.* with products or photo-fragments) can bias the rate coefficients derived from absolute methods to higher values. In the study of Nielsen *et al.* (the only one to report a negative dependence of k_4 on temperature), the pulse-radiolysis technique generated not only very high concentrations of OH ($\sim 10^{13}$ molecule cm^{-3}) but also would have caused substantial fragmentation of CH_3ONO_2 (*e.g.* to CH_3O and NO_2). This probably explains the very large rate coefficient and anomalous temperature dependence observed.

The other temperature-dependent studies report a positive dependence on temperature, with values of E/R (in K) varying from −1054 (this work) to −1020 (Talukdar *et al.*[8]) and −604 (Shallcross *et al.*[11]). While the two studies using the "wall-free" method of PLP–PLIF agree extremely well, the flow tube study of Shallcross *et al.* has a substantially weaker dependence on temperature. Close examination of their data set (5 data points all at $T > 298$ K) reveals considerable scatter in k_4, which is also seen in their plots of k' *versus* [CH_3ONO_2]. We speculate that the difference in slope reflects changes in the wall loss rates of OH, which were determined at room temperature only. As mentioned above, absolute rate studies of slow reactions require that very pure samples are used. In this study and that of Talukdar *et al.*,[8] spectroscopic checks were made to exclude the presence of specific reactive impurities. In the studies of Gaffney *et al.*[9] and Shallcross *et al.*,[11] the sample purity was determined to be > 99%, but no attempt was made to detect impurities such as HNO_3, NO_2 or CH_3OH. Perhaps more pertinent however, is the fact that the two studies that utilized *in situ* (optical absorption) measurement of CH_3ONO_2 are in excellent agreement. *In situ* measurement of the concentration of the excess reactant removes uncertainty associated with calculating [CH_3ONO_2] from partial flows, pressures and variations in the mixing-ratios in storage bulbs. The fact that both this work and Talukdar *et al.*[8] measured absorption cross-sections for CH_3ONO_2 at 213.86 nm that are in almost perfect agreement strongly suggests that the excellent agreement in the values of k_4 reported by these two groups is not fortuitous, but a result of multi-diagnostics and careful execution of the experiments, leading to derivation of the true rate coefficient.

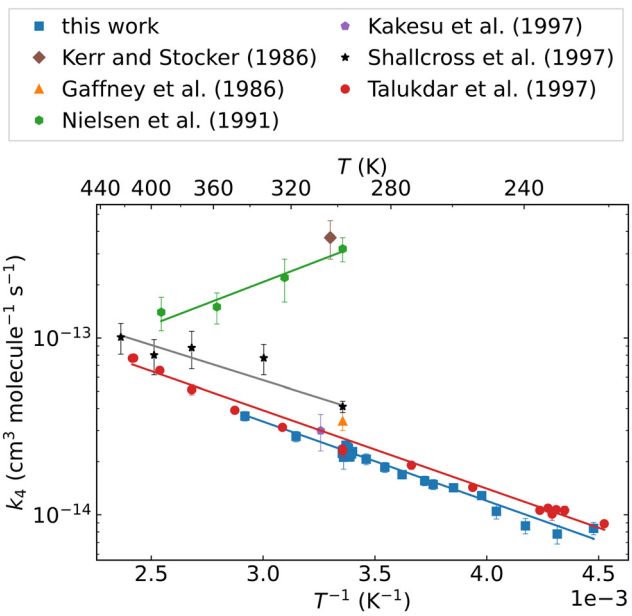

Fig. 7 Arrhenius plot of k_4 *versus* inverse temperature. The rate coefficients and experimental conditions of the present work can be found in Table 3.

Relative rate coefficient measurements. In principle, the relative rate measurements (all close to room temperature) should not be biased by reactive impurities in the CH_3ONO_2 sample, yet the results of the three relative-rate studies are highly divergent. The very large rate coefficients measured by Nielsen *et al.*[10] and Kerr and Stocker[20] can be traced back to an inappropriate choice of reference reactants, which ideally should react with rate coefficients that are similar to the target molecule. The use of 2-methylpropane ($k_{OH+2\text{-methylpropane}}$ = 2.1×10^{-12} cm^3 molecule^{-1} s^{-1} [5]) and ethene ($k_{OH+ethene}$ = 7.8×10^{-12} cm^3 molecule^{-1} s^{-1} at 1 bar[5]) by Nielsen *et al.*[10] and Kerr and Stocker,[20] respectively, would have made relative depletion rates of the reference and target molecule difficult to measure and also prone to other loss processes of CH_3ONO_2. In the relative rate study of Kakesu *et al.*,[3] the more slowly reacting reference trace-gases, methane ($k_{OH+methane}$ = 6.4×10^{-15} cm^3 molecule^{-1} s^{-1} [5]) and ethane ($k_{OH+ethane}$ = 2.4×10^{-13} cm^3 molecule^{-1} s^{-1} [5]) were used. Those authors derived a rate coefficient at 307 K of $(3.0 \pm 0.7) \times 10^{-14}$ cm^3 molecule^{-1} s^{-1}. Within combined uncertainty, this value agrees with the absolute rate coefficient derived in the present study for the same temperature: of k_4(307 K) = $(2.7 \pm 0.4) \times 10^{-14}$ cm^3 molecule^{-1} s^{-1}.

Atmospheric lifetime of CH_3ONO_2 with respect to reaction with OH. As the rate coefficient for the title reaction is independent of pressure under all conditions of the Earth's lower atmosphere (*i.e.* the troposphere and lower stratosphere) we use the Arrhenius expression derived from our experiments using HONO as OH source: $k_4(T) = 7.5 \times 10^{-13} \exp(-1034/T)$ to calculate the lifetime of CH_3ONO_2 with respect to OH loss. For this we assume an altitude independent, global mean OH concentration of 1×10^6 molecule cm^{-3}.[21] The lifetime of CH_3ONO_2 w.r.t. OH reaction at different altitudes is plotted in Fig. S5 (ESI†) and varies from *circa* 500 days at ground level to $>$ 1000 days at 10 km. Photolysis rate coefficients for CH_3ONO_2 vary from $\sim 3 \times 10^{-7}$ s^{-1} to 5×10^{-7} s^{-1} in the boundary layer and lower stratosphere,[15] respectively, resulting in lifetimes with respect to photodissociation of close to 1 month. Our data thus confirms the conclusion of Talukdar *et al.*[15] showing that reaction with OH is a minor sink of CH_3ONO_2 in the atmosphere. This is in contrast to the conclusions of Nielsen *et al.*[10] and Kerr and Stocker[20] who (based on too-high rate coefficients) suggested that reaction with OH is important.

4 Conclusions

Motivated by greatly divergent reports of the rate coefficient for the reaction of OH with CH_3ONO_2, we have determined the rate coefficient using pulsed laser photolysis-laser induced fluorescence. High-quality kinetic data were obtained when measures were taken to avoid the photolysis of CH_3ONO_2. Our result, a positive dependence of the rate coefficient on temperature described by $k_4(T) = 7.5 \times 10^{-13} \exp[(-1034 \pm 40)/T]$, is in close agreement with that reported by Talukdar *et al.*.[8] Both studies used *in situ* measurement of $[CH_3ONO_2]$ using independently determined absorption cross-sections that agreed with 1.2%. The divergent results obtained by other groups are rationalised in terms of choice of OH source or reference reactant and data corrections.

Author contributions

This work was carried out as part-fulfilment of CF's master's degree in chemistry at the Julius-Maximilians-University, Würzburg, Germany. CF and FB conducted the experiments, CF evaluated the data and prepared the manuscript. JC conceptualized the experiment, JC and JL contributed to writing the manuscript.

Conflicts of interest

There are no conflicts to declare.

Acknowledgements

Open Access funding provided by the Max Planck Society.

Notes and references

1 J. M. Roberts, *Atmos. Environ., Part A*, 1990, **24**, 243.
2 E. Atlas, *Nature*, 1988, **331**, 426.
3 M. Kakesu, H. Bandow, N. Takenaka, Y. Maeda and N. Washida, *Int. J. Chem. Kinet.*, 1997, **29**, 933.
4 N. L. Ng, S. S. Brown, A. T. Archibald, E. Atlas, R. C. Cohen, J. N. Crowley, D. A. Day, N. M. Donahue, J. L. Fry, H. Fuchs, R. J. Griffin, M. I. Guzman, H. Herrmann, A. Hodzic, Y. Iinuma, J. L. Jimenez, A. Kiendler-Scharr, B. H. Lee, D. J. Luecken, J. Mao, R. McLaren, A. Mutzel, H. D. Osthoff, B. Ouyang, B. Picquet-Varrault, U. Platt, H. O. T. Pye, Y. Rudich, R. H. Schwantes, M. Shiraiwa, J. Stutz, J. A. Thornton, A. Tilgner, B. J. Williams and R. A. Zaveri, *Atmos. Chem. Phys.*, 2017, **17**, 2103.
5 IUPAC, Task Group on Atmospheric Chemical Kinetic Data Evaluation, (Ammann, M., Cox, R.A., Crowley, J.N., Herrmann, H., Jenkin, M.E., McNeill, V.F., Mellouki, A., Rossi, M. J., Troe, J. and Wallington, T. J.). Last access Sept. 2023, (**https://iupac.aeris-data.fr/**).
6 N. Butkovskaya, A. Kukui and G. Le Bras, *J. Phys. Chem. A*, 2012, **116**, 5972.
7 F. Flocke, E. Atlas, S. Madronich, S. M. Schauffler, K. Aikin, J. J. Margitan and T. P. Bui, *Geophys. Res. Lett.*, 1998, **25**, 1891.
8 R. K. Talukdar, S. C. Herndon, J. B. Burkholder, J. M. Roberts and A. R. Ravishankara, *J. Chem. Soc., Faraday Trans.*, 1997, **93**, 2787.
9 J. S. Gaffney, R. Fajer, G. I. Senum and J. H. Lee, *Int. J. Chem. Kinet.*, 1986, **18**, 399.
10 O. J. Nielsen, H. W. Sidebottom, M. Donlon and J. Treacy, *Chem. Phys. Lett.*, 1991, **178**, 163.

11 D. E. Shallcross, P. Biggs, C. E. Canosa-Mas, K. C. Clemitshaw, M. G. Harrison, M. Reyes López Alañón, J. A. Pyle, A. Vipond and R. P. Wayne, *J. Chem. Soc., Faraday Trans.*, 1997, **93**, 2807.
12 M. Wollenhaupt, S. A. Carl, A. Horowitz and J. N. Crowley, *J. Phys. Chem.*, 2000, **104**, 2695.
13 W. D. Taylor, T. D. Allston, M. J. Moscato, G. B. Fazekas, R. Kozlowski and G. A. Takacs, *Int. J. Chem. Kinet.*, 1980, **12**, 231.
14 J. G. Calvert and J. N. J. Pitts, *Photochemistry*, J. Wiley, New York, 1966.
15 K. R. Talukdar, J. B. Burkholder, M. Hunter, M. K. Gilles, J. M. Roberts and A. R. Ravishankara, *J. Chem. Soc., Faraday Trans.*, 1997, **93**, 2797.
16 C. B. M. Groß, T. J. Dillon, G. Schuster, J. Lelieveld and J. N. Crowley, *J. Phys. Chem. A*, 2014, **118**, 974.
17 G. L. Vaghjiani and A. R. Ravishankara, *J. Chem. Phys.*, 1990, **92**, 996.
18 A. P. Black and F. H. Babers, *Org. Synth.*, 1939, **19**, 64.
19 W. Tsang and R. F. Hampson, *J. Phys. Chem. Ref. Data*, 1986, **15**, 1087.
20 J. A. Kerr and D. W. Stocker, *J. Atmos. Chem.*, 1986, **4**, 253.
21 J. Lelieveld, S. Gromov, A. Pozzer and D. Taraborrelli, *Atmos. Chem. Phys.*, 2016, **16**, 12477.
22 O. J. Nielsen, H. W. Sidebottom, M. Donlon and J. Treacy, *Chem. Phys. Lett.*, 1991, **178**, 163.
23 D. Shallcross, C. Canosa-Mas, K. Clemitshaw, M. Harrison, J. Pyle and R. Wayne, *J. Chem. Soc., Faraday Trans.*, 1997, **93**, 2807.

